Author Manuscript

Author Manuscript

Author Manuscript

Author Manuscript

HHS Public Access

Author manuscript

Biomaterials. Author manuscript; available in PMC 2017 June 01.

Published in final edited form as:

Biomaterials. 2016 June ; 91: 166–181. doi:10.1016/j.biomaterials.2016.03.014.

ECM hydrogel for the treatment of stroke: Characterization of the host cell infiltrate

Harmanvir Ghuman[a,b], **Andre R. Massensini**[a,c,f], **Julia Donnelly**[d], **Sung-Min Kim**[b], **Christopher J. Medberry**[a,b], **Stephen F. Badylak**[a,b,e], and **Michel Modo**[a,b,c,*]

[a]McGowan Institute for Regenerative Medicine, University of Pittsburgh, Pittsburgh, PA, USA

[b]Department of Bioengineering, University of Pittsburgh, Pittsburgh, PA, USA

[c]Department of Radiology, University of Pittsburgh, Pittsburgh, PA, USA

[d]Department of Biological Sciences, University of Pittsburgh, Pittsburgh, PA, USA

[e]Department of Surgery, University of Pittsburgh, Pittsburgh, PA, USA

[f]Universidade Federal de Minas Gerais, Department of Physiology and Biophysics, Belo Horizonte, Brazil

Abstract

Brain tissue loss following stroke is irreversible with current treatment modalities. The use of an acellular extracellular matrix (ECM), formulated to produce a hydrogel in situ within the cavity formed by a stroke, was investigated as a method to replace necrotic debris and promote the infiltration of host brain cells. Based on magnetic resonance imaging measurements of lesion location and volume, different concentrations of ECM (0, 1, 2, 3, 4, 8 mg/mL) were injected at a volume equal to that of the cavity (14 days post-stroke). Retention of ECM within the cavity occurred at concentrations >3 mg/mL. A significant cell infiltration into the ECM material in the lesion cavity occurred with an average of ~36,000 cells in the 8 mg/mL concentration within 24 h. An infiltration of cells with distances of >1500 μm into the ECM hydrogel was observed, but the majority of cells were at the tissue/hydrogel boundary. Cells were typically of a microglia, macrophage, or neural and oligodendrocyte progenitor phenotype. At the 8 mg/mL concentration ~60% of infiltrating cells were brain-derived phenotypes and 30% being infiltrating peripheral macrophages, polarizing toward an M2-like anti-inflammatory phenotype. These results suggest that an 8 mg/mL ECM concentration promotes a significant acute endogenous repair response that could potentially be exploited to treat stroke.

*Corresponding author. University of Pittsburgh, McGowan Institute for Regenerative Medicine, 3025 East Carson St, Pittsburgh, 15203, PA, USA. ; Email: modomm@upmc.edu (M. Modo)

Authors' contribution

HG performed MCAo and implantation surgery, immunohistochemistry, acquired images, phenotype analysis and assisted in drafting the manuscript. AM designed the study, performed MCAo and implantation surgery, performed MRI scanning and immunohistochemistry. JD performed immunohistochemistry and cell phenotype counting. TK performed immunohistochemistry and measurements of cell invasion. CM conceived of the study and provided ECM material for implantation. SFB conceived of the study, provided funding, and assisted with manuscript editing. MM conceived of the study, provided funding, supervised experiments and analyses, and drafted the manuscript. All authors read and approved the final version of the manuscript.

Disclosure

The authors have no personal financial or institutional conflict of interest in any of the drugs, materials, or devices described in this article.

Author Manuscript Author Manuscript Author Manuscript Author Manuscript

Keywords

Biomaterial; Delivery; Extracellular matrix; Injection; Magnetic resonance imaging; Stereotactic; Brain; Stroke; Hydrogel; Phenotypes; Neural progenitor; Macrophage

1. Introduction

Stroke affects approx. 800,000 Americans each year and remains the main cause of adult disability [1]. Unfortunately, very little progress has been achieved in the treatment of chronic stroke [2]. Physical therapy remains the only approved intervention aimed at improving behavioral impairments. However, these improvements are modulated through brain plasticity in existing brain circuitry [3], not through replacing lost cells or tissue. Consequently, the survivors remain severely impaired and typically unable to care for themselves. However, regenerative medicine approaches are being pursued [4], most notably, the intracerebral transplantation of neural stem cells into damaged tissue in an effort to improve behavioral outcomes. However, no replacement of lost tissue has been shown following stroke [5,6], and a large tissue cavity remains in stroke survivors [7].

Provision of a scaffold for implanted cells, either in the form of microparticles or hydrogels, can fill the cavity and promote interactions between the implanted materials and the host brain tissue [8–11]. In normal CNS and non-CNS tissue, the extracellular matrix (ECM) occupies the intercellular space [12]. Decellularization of any tissue produces cell free ECM that can be subsequently formulated as a hydrogel for injection [13]. Such a material can act as a scaffold support for injected neural stem cells in a stroke cavity [10]. In vitro, the chemoattractant cues and differentiation stimuli in ECM harvested from different organ systems, such as the brain, spinal cord and urinary bladder (UBM), influence neural stem cells' phenotypic fate, as well as cell invasion [3–5]. Interestingly, UBM-derived ECM promotes greater neurite outgrowth than CNS-derived ECM [14].

ECM is known to have inductive properties and is widely used as an acellular material to reconstruct functional soft tissue [15]. This repair is mediated through an infiltration of immune cells, such as macrophages, which are activated by the ECM material toward an M2-like, anti-inflammatory phenotype [16,17]. The macrophage phenotype transition is mediated via ECM degradation products and involves the COX1/2 intracellular signaling pathway [18]. In addition, ECM degradation products attract host stem/progenitor cells [19–21]. ECM hydrogels provide both the appropriate mechanical properties and signaling molecules to attract the resident host cells, and obviate the need for exogenous cells [21,22]. These processes are consistent across a range of soft tissue defects [15]. It is therefore plausible that an acellular ECM hydrogel can activate endogenous repair processes, such as neurogenesis, that can potentially be harnessed to support tissue reconstruction in the stroke-damaged brain.

We have previously shown that a reliable delivery and gelation of ECM biomaterial into the stroke cavity can be achieved under MRI-guidance [22,23]. Gelation and retention of ECM hydrogel within the tissue defect was dependent on its concentration. Poor gelation and retention was observed with concentrations of <3 mg/mL, whereas higher concentrations

Author Manuscript Author Manuscript Author Manuscript Author Manuscript

showed good retention and coverage of the lesion cavity. Concentration of ECM therefore influences the rheological properties of the injected material [22,24], which is known to affect the differentiation of neural stem cells in vitro [25–27] and potentially can also affect cell invasion [28]. However, ECM concentration also determines the abundance of inductive signals, which can influence the phenotype, as well as the number, of invading cells [17]. Based on these potential differences in rheological and inductive properties of different concentrations of ECM, we investigated the quantity and phenotype of cells that infiltrate a UBM-derived ECM following implantation into an experimentally-induced stroke cavity in a rat model.

2. Methods

2.1. Extracellular matrix (ECM) hydrogel

To produce a ECM hydrogel, the basement membrane and tunica propria of an adult porcine urinary bladder (Tissue Source, Inc., Lafayette, IN) were isolated by mechanical delamination, as previously described [24]. Decellularization was performed using 0.1% peracetic acid in 4% ethanol (v/v; 120 min; 300 rpm) with agitation. A series of PBS and deionized water rinses removed cellular debris. Decellularization was confirmed using Hematoxylin & Eosin, 4′,6-diamidino-2-phenylindole (DAPI) staining, agarose gel electrophoresis, and quantification of remnant DNA [29]. The remaining ECM was lyophilized, comminuted, and solubilized with pepsin (1 mg/mL) in 0.01 N HCl. pH neutralization was achieved by addition of 0.1 N NaOH. This preparation contains 129 proteins that are predominantly of cytoplasmic (39%) and ECM (14%) origin, with 14% being secreted cytokines, 19% involved in cytoskeletal processes, 13% in cell adhesion and only a small fraction (1%) in a stimulatory and remodeling role [30]. The 10 most abundant molecules found within this preparation are: filamin-A, myosin-11, desmin, myosin-9, filamin-C, alpha-actinin-1, lamin-A.C, desmoplakin, actin, collagen VI. A complete list with MOWSE protein scores can be found in Ref. [30]. Approximately 70% of the overall material is collagen [13], but other prominent ECM proteins, such as fibronectin, decorin, laminin subunit γ1 are also present [30]. A variety of growth factors are also retained within the ECM preparation, including Transforming growth factor-β, vascular endothelial growth factor-A, basic fibroblast growth factor, and nerve growth factor [31], which all are known to influence neuronal and endothelial cells.

Dilution to a desired concentration (1, 2, 3, 4, 8 mg/mL) was attained by suspension in the appropriate volume of PBS [24]. Gelation of this preparation is concentration- and temperature-dependent with concentrations < 3 mg/mL not forming a hydrogel, as previously described in detail [13,22]. A 4 mg/mL preparation takes 3.2 min to reach 50% gelation and achieves a viscosity of 0.084 Pa s, whereas an 8 mg/mL is more than 4 times higher at 0.443 Pa s and only takes 3 min to reach 50% gelation. The storage modulus (G′) for 4 mg/mL (76.6 Pa) and 8 mg/mL (460.4 Pa) exceeded their loss modulus (G″, 11.0 Pa; 66.4 Pa). An 8 mg/mL preparation was the highest concentrations that was prepared for this study [22] and approximated the reported 500–1000 Pa elastic modulus of brain tissue [32–34]. A 0 mg/mL condition consisting of only PBS served as a control.

Author Manuscript Author Manuscript Author Manuscript Author Manuscript

2.2. Middle cerebral artery occlusion (MCAo)

All animal procedures complied with the US Animals Welfare Act (2010) and were approved by the University of Pittsburgh Institutional Animal Care and Use Committee (IACUC). Sprague-Dawley rats (male, 260 ± 15 g, Taconic Labs, USA) were maintained on a 12-h light/dark schedule, with food and water available *ad libitum*. For transient intraluminal right middle cerebral artery (MCA) occlusion, a rat model of stroke, a 5-0 silicon rubber-coated monofilament (diameter 0.12 mm, length 30 mm, tip coating at 0.35 mm for 5–6 mm, 503556PK10, Doccol, USA) was advanced to the ostium of the MCA in the circle of Willis under isoflurane (4% induction, 1% maintenance in 30% O_2) anesthesia. The MCA was occluded for 70 min prior to reperfusion by retracting the filament to the common carotid bifurcation. After recovery from anesthesia, animals were assessed for forelimb flexion and contralateral circling with daily post-operative care and neurological assessment until they recovered pre-operative weight [35,36].

2.3. Magnetic resonance imaging (MRI) and infarct volume calculation

To assess the presence, location and volume of tissue loss, MCAo rats were anesthetized with isoflurane (4% induction, 1% maintenance) and scanned using a T_2-weighted spin-echo MRI sequence (TR = 6000 ms, TE = 8 ms, 8 Averages, FOV 30 × 30 mm, 128 × 128 matrix, 42 slices at 0.5 mm thickness) on a horizontal bore 9.4 T Varian scanner 12 days post-infarction. Stroke-damage was defined as tissue with a hyperintense signal on T_2-weighted images that were thresholded at 1 standard deviation above the mean of a rectangular region of interest (ROI) in the contralateral hemisphere, encompassing striatum, corpus callosum and neocortex [37,38]. Rats (n = 30) with lesion volume >40 mm^3 (i.e. 40 μL) were selected for injections by random assignment to treatment groups, resulting in equivalent distribution of lesion volumes across all groups with lesion volumes ranging from 40 to 290 μL (Supplementary Fig. 1A).

2.4. Implantation procedure

Fourteen days post-stroke, rats were subjected to the ECM implantation procedure by placement into a stereotactic frame (Kopf, USA) under isoflurane anesthesia (4% induction, 1% maintenance in 30% O_2). A vertical skin incision exposed Bregma on the skull and provided guidance for the location of Burr holes for the placement of a 250 μL Hamilton syringe with a 24 G beveled tip metal needle (Hamilton) filled with solubilized ECM, as well as a hole for a drainage cannula (24 G) [22]. Ideally, a needle with a very small bore size is used for injection of biomaterials to minimize injection damage to intact or damaged brain tissue [23]. Nevertheless, the potential aggregation and gelation of biomaterials can obstruct the needle lumen and hence a large needle size (24 G) is required to ensure the efficient delivery of material, as well as minimize damage to brain tissue [39]. MR images of lesion location and volumes were used to define stereotactic coordinates for needle/cannula placements [22,23]. Needles/cannula were slowly lowered into brain tissue. Lesion-equivalent volumes of solubilized ECM (40–290 μL) were injected into the ventral posterior region of the cavity and volume displaced the less dense necrotic debris, whereas drainage was achieved at the most dorsal part of the lesion [22]. We have previously demonstrated that a precise neurosurgical planning is required for these large volume injections to avoid

Author Manuscript Author Manuscript Author Manuscript Author Manuscript

misplacement or leaching of material into the lateral ventricles, but also to avoid damage to structures in the path of injection [22]. Injection of ECM biomaterial (0, 1, 2, 3, 4, 8 mg/mL concentrations, n = 5 per condition) was controlled using a frame mounted injection pump (World Precision Instruments, USA) at a constant speed of 10 μL/min until the total volume was delivered (4–29 min). The needle and cannula were left in place for 5 min to allow material to dissipate and gel before it was slowly removed from the brain. The solubilized ECM formed a hydrogel in situ as it assumed 37 °C body temperature. Burr holes were filled with bone wax (Fisher) prior to suturing. LX4 (Ferndale, containing 4% Lidocaine) was topically applied as an analgesic.

2.5. Histological assessment

2.5.1. Perfusion and immunohistochemistry—To analyze the distribution of the ECM hydrogel and the acute cell infiltration within the hydrogel, 1 day post-implantation rats were transcardially perfused with 0.9% saline followed by 4% paraformaldehyde (in 0.2 M PBS) to fix brain tissue prior to its removal from the skull. Brains were post-fixed in 4% paraformaldehyde for 24 h prior to being cryopreserved in 30% sucrose with sodium azide (Sigma) at 4 °C. Histological sections (50 μm thickness) were cut on a cryostat (Leica) directly onto microscopic slides. Brain sections were washed 3 × 10 min with 0.01 M PBS, followed by 1 h permeabilization in PBS + 0.1% Triton X-100 (Sigma) at room temperature (21 °C). Sections were then washed 3 × 10 min in PBS × 0.05% Triton X-100 followed by one hour in blocking solution (PBS + 0.05% Triton X-100 + 10% Normal Goat Serum, NGS, Vector). Primary antibodies (Supplementary Table 1) were then applied, diluted in blocking solution (0.05% Triton X-100, 10% NGS in PBS) and incubated at 4 °C overnight. After rinsing of the primary antibodies (3 × 5 min PBS), appropriate secondary AlexaFluor 488, 555, or 633 antibodies (Life Technologies) were applied for 1 h prior to 3 × 5 min. washes in PBS. Finally, sections were coverslipped with Vectashield for fluorescence containing DAPI (Vector Laboratories) and stored at 4 °C prior to imaging. Visualization of antibodies was performed with a fluorescence microscope (Axioimager M2, Zeiss) interfaced with a monochrome camera driven by Stereo Investigator image capture software (MBF Bioscience) using a motorized stage and the Virtual tissue module to tile individual 10× images into whole hemisphere images.

2.5.2. Cell invasion – quantification—To quantify the number and distribution of cells infiltrating the ECM hydrogel, a semi-automated script (Lux64R) was used. Collagen I immunolabeling delineated the ECM hydrogel (Fig. 1A) against host brain tissue [22] creating a mask (Fig. 1B) that was used to define the region of interest (ROI) within which individual cell nuclei were identified based on DAPI staining using a threshold and size definition. A colorimetric scale ranging from blue, for cells most proximal, to red, indicating cells most distant from the adjacent host tissue, was used to create a color map of cell invasion (Fig. 1C), while providing measurements of distance of individual invading cells (Fig. 1D). The tangent distance of infiltration from the cavity boundary was measured for each cell using the cavity's center of mass as reference. To reveal a relationship between ECM hydrogel concentration and cell invasion, 25 μm concentric bins were used to compare the number and distance of invading cells in relation to center of mass for each defect. It is important to note that individual shapes of cavities were different, some more irregular than

Author Manuscript Author Manuscript Author Manuscript Author Manuscript

others. In some cases, the center of mass is hence not the most accurate point of reference towards which the cells infiltrated, but was still the most pertinent to afford a grouping of cell invasion and provide a comparison. Validation of this approach was shown by the high correlation (>95%) between manual counting and distance measurements against the semi-automated approach (Fig. 1E). All tissue slices covering the stroke lesion were included in this analysis (Fig. 2A).

2.5.3. Cell infiltration – cell phenotype analysis—To determine the phenotype of cells invading the injected ECM, collagen I was used to delineate the border between host and biomaterial. Animals injected with concentrations >3 mg/mL resulted in a gelation and retention within the cavity (Fig. 2A). Lower concentrations showed small patches of material in the cavity, typically attached to remnants of damaged tissue [22]. Due to differences in the extent of material present within a given defect, the number of fields of view (FOVs) counted ranged from 5 to 15 images to cover the material present within the cavity (Fig. 2B). Where ECM hydrogel covered the whole defect (i.e. concentrations of ≥3 mg/mL), FOVs were equally spaced throughout the material within a section and counted across all anterior-posterior slices. For analysis of cell phenotypes of invading cells, the total number of cells (i.e. Hoechst+) within a FOV of the ECM material were counted. Phenotypic markers for neural progenitor cells (doublecortin, DCX), astrocytes (glial fibrillary acid protein, GFAP), oligodendrocytes (2′,3′-cyclic-nucleotide 3′-phospodiesterase, CNPase), endothelial cells (rat endothelial cell antigen 1, RECA-1), microglia (ionized calcium-binding adapter molecule 1, Iba-1), as well as macrophage activation (CD206 for the M2 phenotype, CD86 for M1 phenotype). Although many mononuclear macrophages share histological markers, Iba-1 is considered a fairly specific marker of brain microglia [40]. The phenotype of invading cells was determined by counting the number of cells positive for a given marker within a FOV (Fig. 2C). To account for differences in the number of invading cells, phenotypes were expressed as % of total cells present within a FOV. An average of 200 cells were analyzed per FOV (range 10–600 cells).

2.6. Statistical analyses and contour plots

Statistical analyses were performed in SPSS 17 for Mac (IBM) with significance set at $p < 0.05$. Specifically, a two-way ANOVA was used to compare cell invasion and the number of cells within each annulus, using a Bonferroni post-hoc test to validate significant comparisons. A one-way ANOVA with Bonferroni post-hoc testing was used to contrast the effects of ECM concentration on different cell phenotypes, as well as a comparison between lesion volumes and total cell invasion. The different ECM concentrations and the variance in MRI lesion volumes complied with a factorial design (also known as Design of Experiment, DoE) that is built on the foundation of analysis of variance by using independent variables that allowed us to systematical determine their effect on measured data (i.e. the dependent variable), such as cell invasion, to generate contour plots (Minitab 8). These contour plots provided an overview of the entire experimental space of these variables allowing us to determine potential effects of intermediary concentrations or lesion volumes on the dependent variables. Graphs were drawn in Prism 6 (GraphPad) with data point representing the mean and bars reflecting the standard deviation.

Author Manuscript Author Manuscript Author Manuscript Author Manuscript

3. Results

3.1. Host tissue-ECM hydrogel interface

Injection of ECM precursor gel into the lesion cavity resulted in gelation of material at concentrations >3 mg/mL. This in situ gelation resulted in the creation of an interface between the ECM hydrogel and the host tissue (Fig. 3). However, stroke created a complex array of microenvironments of which cavitation is the most severe form of damage. Adjacent to the cavity, tissues void of neuronal cells and undergoing astrocytosis can be found. In some cases, an ongoing macrophage response can be seen that clears cellular debris and eventually removes extracellular matrix (i.e. the process of tissue cavitation). At concentrations >3 mg/mL a clear interface between the hydrogel and host tissue was evident and peri-cavity cortex was often severely damaged. ECM gel precursor in some instances permeated into these areas.

Microglia, macrophages and astrocytes can be found in large abundance around the lesion cavity and in areas of tissue damage. With 0 mg/mL, a high cellular density of microglia and astrocytes can be seen around the lesion cavity forming a scar, i.e. glia limitans, that defines the boundary between tissue and cavity (Fig. 4). This interface is somewhat preserved at the lower concentration of ECM precursor gel (1 & 2 mg/mL), with some ECM forming small patches of gel at the tissue boundary agglomerating around tissue remnants within the cavity. Small numbers of microglia and astrocytes can be found within this injected ECM. At higher concentrations, where gelation of ECM occurred within the cavity, a more distinct interface with host tissue can be identified. A significant infiltration of host cells was observed, especially in areas where cavitation was small. At concentrations of 4 and 8 mg/mL, a well-defined delineation between ECM hydrogel and tissue can be observed, but host cell invasion was also evident.

3.2. ECM hydrogel cell infiltration

Both structural support and inductive cues are necessary for cells to migrate into the ECM biomaterial. Where there is a close interface between ECM hydrogel and the host tissue (Fig. 5A), cells infiltrated the material and migrated inward. Host cell infiltration was also observed across small gaps between the ECM hydrogel and host tissue (Fig. 5B). However, these gaps are potentially artifacts of a differential fixation of tissue and hydrogel. Cell infiltration often followed a chain-like path that trailed channels within the collagen I staining found in the ECM hydrogel. Commonly the cells with the deepest infiltration distance were microglia (Iba-1+), with astrocytes (GFAP+) being found closer to host tissue (Fig. 5C). The availability of these cells at the tissue interface (i.e., the glial scar) may position these cells in a prime location for this acute (24 h) invasion. Infiltrating cells may form pathways along which other cells pursue their infiltration (Fig. 5D). It is unclear, however, if some cells remain in place or if all cells continue infiltration towards the center of mass (and beyond).

To illustrate the patterns of cell invasion, heat maps of individual nuclei and their distance of invasion were generated. It was evident here that lower concentrations, where no gelation and no significant retention of ECM material occurred, very few cells were present in the

Author Manuscript Author Manuscript Author Manuscript Author Manuscript

ECM material. Concentrations >3 mg/mL of ECM hydrogel resulted in large numbers of infiltrating cells (Fig. 6A). A comparison of anterior-posterior colorimetric maps indicated that cavity shape influenced cell invasion, with shorter distances between host tissue boundaries being more completely covered compared to greater distances, as found in the central slice of the cavity (Fig. 6B). Nevertheless, this acute 24 h infiltration pattern resulted in some cases with complete invasion of the material. A good interface between host and ECM material in itself is not the only determinant in the distance of infiltration. In some case, there was evidence of infiltration into the material, but patches within the ECM hydrogel were not uniformly infiltrated ("blind spots"), whereas other adjacent patches showed a strong infiltration (Fig. 6C). These "blind" patches were also evident where there was a good interface between host-ECM (Fig. 6D). Other cases showed that the adjacent host tissue might not respond to the ECM (Fig. 6E and F). In some cases, small channels of cells migrated towards the center of mass without there being an equal distribution of cells throughout the material (Fig. 6G). Preferential routes of colonization of the ECM are hence potentially important considerations in how host cells invade the material (Fig. 6Gi).

To provide a quantitative comparison of cell invasion, the number of cells contained in concentric 25 μm from the host tissue edge to the center of mass of the ECM hydrogel were plotted to reveal total cell invasion for each concentration. The highest number of invading cells was found with 8 mg/mL (average of 36,628 cells), followed by a similar amount of cells at 4 mg/mL, with significantly fewer cells invading at 3 mg/mL ($p < 0.05$) (Supplementary Fig. 1B). There were very few cells invading the cavity in concentrations <3 mg/mL and none in the 0 mg/mL (as there was no identifiable ECM material present for invasion) ($p < 0.001$). The distance of invasion within 24 h revealed cells invading the 8 mg/mL ECM hydrogel by >1500 μm of which >5500 cells were within the first 25 μm of ECM hydrogel (Fig. 7A). A cellular infiltration speed of 62.5 μm/h can hence be calculated. The degree and distance of cells infiltrating at 3 mg/mL was markedly less than at 4 or 8 mg/mL ($p < 0.01$). Indeed, one animal showed very little infiltration at 3 mg/mL, but another showed an infiltration equivalent to those at higher concentrations (Fig. 7B). Also at 4 mg/mL, some variability in the degree and distance of cell infiltration was observed between different animals (Fig. 7C), further highlighting that factors beyond the concentration of the ECM and its gelation within the cavity influence cell invasion. The 8 mg/mL concentration performed the most consistently with all animals showing a good infiltration of cells (Fig. 7D), possibly reflecting a mass effect that this concentration exerts on host tissue, creating a more consistent and well defined interface.

3.3. Lesion volume and ECM concentration influence cell invasion

Although it is evident that concentration is a major determinant of cell invasion, lesion volume is also likely to be a major contributing variable. Indeed, all conditions, in which there was good retention of material within the lesion cavity (>3 mg/mL), showed a relationship between the size of defect and the number and distance of cells invading ($r > 0.8$ for both, Supplementary Table 2). The larger the deficit (and hence the larger injected volume of ECM), the greater the number of cells that infiltrated the material and the greater the distance of infiltration. At lower concentrations, no relationship was evident, as insufficient material was available to warrant significant cell invasion.

Author Manuscript Author Manuscript Author Manuscript Author Manuscript

To determine how different concentrations of ECM influence cell invasion, while accounting for differences in lesion volume, a contour plot was created and showed a more complex relationship between these factors (Fig. 8A). Concentrations <5 mg/mL, showed a poor invasion within 24 h, apart for lesion volumes of 180–220 μL. A peak invasion of cells was observed with an 8 mg/mL concentration of ECM and a narrow lesion volume of 140–150 μL. Although total numbers of invading cells is an important indicator of inductive potential of ECM, larger lesions have more space for greater numbers of cells to invade. Determination of cell density (i.e. invaded cells/μL volume) can mitigate this issue and provide a more accurate description of repopulation, but potentially can be higher in smaller lesions, as there is less space to fill (Fig. 8B). Nevertheless, the overall interaction between ECM concentration and lesion volume was very similar between total cell invasion and cell density, with concentrations of <5 mg/mL having the lowest cell density per area of ECM, apart of the lesion volumes of 180–220 μL, where cell density was slightly elevated for concentrations as low as 3 mg/mL. Higher cell density per area of ECM was found with concentrations >6.5 mg/mL and lesion volumes <240 μL. A peak acute cell density of >500 cells/μL was also associated with an 8 mg/mL concentration and a narrow lesion volume of 140–150 μL.

Another factor affected by ECM concentration and lesion volume is the distance of cell infiltration. A simple correlational analysis indicated a very strong correlation between the lesion volume and the distance of cell infiltration. The distance was very similar for 3, 4 and 8 mg/mL (Supplementary Table 2). Cell invasion distance was also strongly correlated with total cell infiltration for 3 mg/mL ($r = 0.90$, $p < 0.05$), 4 mg/mL ($r = 0.84$, $p = 0.07$), and 8 mg/mL ($r = 0.97$, $p < 0.01$), hence indicating a close relationship and interdependence between these different factors. A contour plot further highlighted this relationship (Fig. 8C), indicating that a concentration of >3 mg/mL is required for any infiltration to occur. Interestingly again, two separate peak spots for cell infiltration >2000 μm occurred, with larger lesions of 180–220 μL requiring lower ECM concentrations (4–5 mg/mL) and smaller lesions of 120–180 μL requiring a higher ECM concentration (>7 mg/mL).

3.4. Phenotypic characterization of cell infiltration

Considering the rapid infiltration of a large number of cells, it is essential to determine the phenotypes of the cells, as well as their participation in the remodeling and repopulation process. Indeed, the chain-like migration of cells along certain tracks within the injected ECM suggests that certain pioneering cells pave the way for others to follow. Iba-1 microglia are very common amongst the cells infiltrating the furthest into the hydrogel (Fig. 9A), with GFAP+ astrocytes being located closer to the host tissue. It is noteworthy that astrocytes and microglia within hydrogel have a more bulbar appearance within the ECM than in native tissue. Interestingly, significant numbers of DCX+ neural progenitors can be found to infiltrate the ECM hydrogel even during this acute phase, as do endothelial cells (Fig. 9B). As these infiltrate the gel, morphologically these appear bulbar and can be contrasted with areas where they show a more mature morphology. The presence of more mature morphologies was typically associated with ECM hydrogel surrounding remnants of damaged tissue (Fig. 9C). Oligodendrocyte progenitors (CNPase+ cells) were also seen to infiltrate the ECM, hence indicating that all resident brain cells can be found to infiltrate

Author Manuscript Author Manuscript Author Manuscript Author Manuscript

ECM hydrogel within 24 h. Nevertheless, the majority of cells found to infiltrate the ECM acutely were monocytes (mostly macrophages) that expressed markers for an M1 (CD86+) and/or M2 (CD206+) phenotype, presumably participating in the remodeling of the ECM.

A quantification of the phenotypes and comparison across ECM concentrations showed that 8 mg/mL recruited the highest percentage of brain-derived cells (Fig. 10). An average of 8% of invading cells at the 8 mg/mL concentration were DCX+ with all other concentrations recruiting <3% of neural progenitors ($p < 0.001$), i.e. the key phenotype required for repopulation of a neural tissue. Surprisingly, the recruitment of astrocytes was equivalent for all groups, as well as being very similar to neural progenitors at lower concentrations. The only slight rise (+1%) in astrocytes' infiltration was seen with 3 mg/mL, but this was statistically (and most likely biologically) insignificant. Oligodendrocytes were the most common "neural"-derived phenotype overall with >5% across all concentrations and a peak of 11% of infiltrating cells at 8 mg/mL ($p < 0.01$). In contrast, very few endothelial cells invaded (<3%), with a peak infiltration seen again with 8 mg/mL (4.5% of cells, $p < 0.05$). As expected, microglia were the most common phenotype of brain-derived cells that infiltrated the ECM with the highest proportion of cells being found at 8 mg/mL ($p < 0.05$). These results indicate that ~60% of cells at 8 mg/mL were derived from the brain, with the lowest proportion (~30%) invading from the surrounding tissue with a concentration of 3 mg/mL. A significant proportion of cells hence infiltrated from outside the brain. Monocyte (microglia/macrophage) polarization contrasting M2 (CD206+), M1 (CD86+), or M2/M1 (CD206+/CD86+) markers indicated that an M1-like phenotype was the most common across all concentrations, but was lowest at 8 mg/mL ($p < 0.01$). The proportion of M2/M1 marker co-expression was also highest at 8 mg/mL ($p < 0.05$), although 3 mg/mL was equivalent. Only M2-like (i.e. CD206+) cells were very scarce with <2% being present at the 8 mg/mL concentration and no significant difference being evident across ECM concentrations.

4. Discussion

Repairing the tissue damage caused by a stroke remains a major challenge that continues to be severely understudied. Indeed, the formation of a cavity at the core of the site of infarction not only results in tissue damage, but a complete loss of tissue [7]. Considering the varied topology of stroke damage, non-invasive image-guided targeting of this area for injection is required [23]. Herein we demonstrate that ECM hydrogel implanted into a chronic stroke lesion 1) induces a host tissue response that leads to a cell infiltration; 2) a structural support is required for cell infiltration into the cavity; 3) rheological properties akin to intact tissue promotes the most significant cell infiltration; 4) a significant portion of infiltrating cells are of a monocyte (i.e. microglia/macrophage) phenotype with a concentration-dependent polarization towards an M2-like phenotype and 5) an 8 mg/mL ECM concentration attracts large numbers of neural and oligodendrocyte progenitors within 24 h.

Author Manuscript Author Manuscript Author Manuscript Author Manuscript

4.1. ECM hydrogel promotes host cell infiltration

Foremost of all, recruitment of host cells into the injected material requires a gelation and retention of material within the cavity. At 1 day post-implantation, a robust formation of the hydrogel can be observed at concentrations >3 mg/mL [22]. However, small agglomerates of ECM at the border of the tissue, as demonstrated here, can also attract host cells, albeit at a smaller scale. Due to the lack of structural support throughout the cavity, no repopulation of the cavity with host cells occurs. In contrast, gelation of the ECM in situ resulted in a very dramatic acute infiltration of cells into the cavity in the order of ~36,000 for the 8 mg/mL ECM concentration. This concentration was rheologically comparable to uninjured brain tissue, with an elastic modulus of 500–1000 Pa [36–38], which could explain why this concentration was so efficient in attracting host cells, specifically neural progenitors and oligodendrocytes. The mechanical properties of the hydrogel play an important part in cell invasion and phenotypic differentiation [25,26] Stiffer gels (1000–10,000 Pa) are associated with astrocytes, whereas softer gels (100–1000 Pa) are more likely to promote neuronal differentiation [41]. An intermediate stiffness (400–800 Pa) provides a mixtures of cells, as was seen here in the 8 mg/mL condition (460 Pa), and could provide mechanical properties that are conducive to neural tissue engineering requiring neurons, astrocytes, as well as oligodendrocytes. However, it should be noted that the mechanical properties of the hydrogel begin to change almost immediately after in vivo placement as a consequence of cell invasion and the onset of degradative processes.

A good interface with host tissue is nevertheless also important. A lack of interface did not result in a good cell infiltration. Even if there was a good interface, in some cases there was a poor invasion. It is conceivable that the density gradient at the interface influences cell infiltration [42], which potentially could be due to tissue characteristics, such as a glia limitans, or hydrogel characteristics, such as a higher material concentration at the cavity edge producing a higher elastic modulus [43]. Although very dense material can invoke a foreign body response in the brain that leads to an encapsulation of material by fibrotic scarring [44], injections of hydrogels typically exhibit a reduced microglia and astrocytes response compared to just needle track damage [43]. Although microglia and astrocytes are abundantly present in the peri-cavity tissue [45], more neurons and oligodendrocytes invaded the ECM hydrogels than astrocytes within 24 h of injection. The reciprocity in interaction between hydrogel and host brain is essential to determine the host tissue response and guide cell invasion or induce further scarring and a foreign body response [46]. Further engineering of hydrogel potentially promises to provide a greater control over this interaction and influence the infiltration of specific cell phenotypes [47].

Apart from the rheological properties, inductive cues provided by the ECM material are thought to be the key mediator of cell infiltration [15]. The 8 mg/mL concentration in the current study was the highest concentration implanted and hence also provided the greatest abundance of inductive cues to elicit a regenerative response [15,48]. Indeed, the injected ECM contains growth factors, such as vascular endothelial growth factor, basic fibroblast growth factor, and nerve growth factor, which can be released from the injected material [30,31]. The released proteins can permeate into host tissue, create a gradient, and facilitates infiltration of host cells, such as microglia/macrophages [49]. It is thought that these

Author Manuscript Author Manuscript Author Manuscript Author Manuscript

immune cells exert a pioneering function in that they invade the ECM, leading a constructive remodeling and in this process create trails of molecules that attract host tissue cells to gradually repopulate the material [46]. Microglia (Iba1+) cells were predominant amongst the cells that infiltrated the furthest into the ECM. Their infiltration appeared to follow a topological trail within the ECM. The chain-like infiltration suggests that there are particular trails within the material that these cells preferential follow, although at the tissue boundary a broader cell invasion into the material is observed. These invasion trails are likely to be a combination of abundant signaling molecules that attract particular cells, as well as conducive mechanical properties, such as gel surface curvature within the injected material, that interact reciprocally with pioneering cells [50].

4.2. Role of cell phenotypes infiltrating into scaffold

Peripheral macrophages are infiltrating the ECM material and it is thought that both macrophages and microglia here exerted very similar functions, notably constructive remodeling of the ECM hydrogel and facilitating the invasion of host organ cells. All ECM concentrations (apart of 0 mg/mL) invoked a macrophage/monocyte infiltration. Proportionally this was lowest at the 8 mg/mL concentration. However, this is due to a greater number of host brain cells infiltration at this concentration, but in absolute numbers leads a similar number of macrophages than at 3 or 4 mg/mL. Although it is conceivable that microglia and macrophage infiltration are a response to recognizing a foreign object, the difference in cell numbers and proportions across the different concentrations indicate that other factors are also important. The stiffness of the injected material, for instance, can influence macrophage infiltration and morphology of these cells, with higher stiffness being associated with a greater response [51]. Although macrophages are involved in a foreign body response to injected material [43], this typically involves macrophages of an M1-like phenotype only [52]. An M1-like phenotype response, in the absence of a polarization towards an M2-like phenotype, is associated with an insufficient decellularization of ECM material [53]. Although the M1-like response here was dominant overall, especially in the 1 mg/mL condition, polarization towards an M2 phenotype, especially at 3 and 8 mg/mL, using the same ECM material, indicates that this was not due to an insufficient decellularization. An M2-like phenotype polarization of invading macrophages has indeed been linked with peripheral nerve repair [54] and the constructive remodeling response of injected ECM [55]. It is this M2-like polarization that is thought to be crucial to attract cells from the host organ to repopulate the tissue defect and eventually replace the injected material with new tissue [15].

The infiltration of microglia and macrophages is thought to be an M1-like response with a shift towards an M2-like phenotype, occurring through juxtacrine or paracrine signaling within the ECM material [49]. It is important to stress that all infiltration into the material, i.e. even macrophage infiltration, was through host tissue, as there were no blood vessels contained within the cavity that would allow a direct infiltration of peripheral macrophages into the hydrogel. It is suggested that the mobilization of host brain cells (neurons, astrocytes, oligodendrocytes) and endothelial cells for infiltration followed a chain-like migration of pioneering microglia and macrophages. This mobilization is a rapid process, as within 24 h here, microglia and macrophages are seen at distances >1500 μm into the

Author Manuscript Author Manuscript Author Manuscript Author Manuscript

hydrogel. Moreover, a high proportion (~10%) of oligodendrocyte and neural progenitor cells was observed to follow these pioneering cells. Indeed, it is remarkable that within such a short time >60% of cells found within the hydrogel were cells required for tissue replacement. Still, it is unclear here why neural and oligodendrocyte progenitors were more abundant in their infiltration than astrocytes and endothelial cells. It is conceivable that this is due to ECM molecules required for migration [56]. Specifically, the abundance of ECM molecules, such as fibronectin and laminin, are thought to be pivotal in a repair response of neural stem cells [57,58] and might explain the relative preferential infiltration of neural and oligodendrocyte progenitors. In contrast, the high collagen content of these ECM hydrogels might serve as a deterrent to astrocytes [59,60], hence at this acute stage leading to a selective preference of neural progenitor infiltration. Nevertheless, the infiltration of a high proportion of neural progenitors is very encouraging to harness endogenous repair mechanisms into the lesion cavity and potentially promote the replacement of lost tissue using inductive biomaterials. Further investigations into the provision of appropriate paracrine and juxtacrine recruitment cues, as well as rheological conditions that are conducive to cell invasion of a neural cell population [25,26,61,62] may enhance this potential.

5. Conclusions

Implantation of ECM gel precursor leads to the in situ formation of a hydrogel at concentrations >3 mg/mL, resulting in its retention within the lesion cavity. The ECM material induces a host response that is characterized by a rapid and robust cell infiltration that is concentration-dependent, but is also influenced by the size of the lesion. ECM concentration further influences the phenotype of cells, with an 8 mg/mL concentration resulting in ~60% of brain-derived cells. This concentration produced the most significant polarization towards an M2-like macrophage phenotype at this acute time point, whereas lower concentrations exerted a less significant M2-like polarization. These results hence suggest that an 8 mg/mL ECM concentration promotes a significant acute endogenous repair response. Nevertheless, a time course study characterizing cell infiltration, ECM remodeling, cell repopulation and its effect on host tissue is required to provide a more comprehensive framework to determine the potential of ECM hydrogel as a potential treatment for chronic stroke.

Supplementary Material

Refer to Web version on PubMed Central for supplementary material.

Acknowledgments

This study was funded by a seed grant from the Department of Health of the Commonwealth of Pennsylvania (4100061184) and the National Institute of Neurological Disorders and Stroke (R01NS08226). ARM was supported by a Fellowship from CAPES Foundation, Brazil. SFB and MM gratefully acknowledge support from Vertex Pharmaceuticals.

Author Manuscript Author Manuscript Author Manuscript Author Manuscript

Appendix A. Supplementary data

Supplementary data related to this article can be found at http://dx.doi.org/10.1016/j.biomaterials.2016.03.014.

References

1. Mozaffarian D, Benjamin EJ, Go AS, Arnett DK, Blaha MJ, Cushman M, et al. Heart disease and stroke statistics–2015 update: a report from the American Heart Association. Circulation. 2015; 131:e29–e322. [PubMed: 25520374]
2. Cumberland Consensus Working G. Cheeran B, Cohen L, Dobkin B, Ford G, Greenwood R. The future of restorative neurosciences in stroke: driving the translational research pipeline from basic science to rehabilitation of people after stroke, Neurorehabil. Neural Repair. 2009; 23:97–107.
3. Dalise S, Ambrosio F, Modo M. Brain plasticity and recovery in preclinical models of stroke. Arch Ital Biol. 2014; 152:190–215. [PubMed: 25987181]
4. Modo M, Ambrosio F, Friedlander RM, Badylak SF, Wechsler LR. Bioengineering solutions for neural repair and recovery in stroke. Curr Opin Neurol. 2013; 26:626–631. [PubMed: 24136127]
5. Smith EJ, Stroemer RP, Gorenkova N, Nakajima M, Crum WR, Tang E, et al. Implantation site and lesion topology determine efficacy of a human neural stem cell line in a rat model of chronic stroke. Stem Cells. 2012; 30:785–796. [PubMed: 22213183]
6. Encarnacion A, Horie N, Keren-Gill H, Bliss TM, Steinberg GK, Shamloo M. Long-term behavioral assessment of function in an experimental model for ischemic stroke. J Neurosci Methods. 2011; 196:247–257. [PubMed: 21256866]
7. Moreau F, Patel S, Lauzon ML, McCreary CR, Goyal M, Frayne R, et al. Cavitation after acute symptomatic lacunar stroke depends on time, location, and MRI sequence, Stroke –. J Cereb Circ. 2012; 43:1837–1842.
8. Park KI, Teng YD, Snyder EY. The injured brain interacts reciprocally with neural stem cells supported by scaffolds to reconstitute lost tissue. Nat Biotechnol. 2002; 20:1111–1117. [PubMed: 12379868]
9. Bible E, Chau DY, Alexander MR, Price J, Shakesheff KM, Modo M. The support of neural stem cells transplanted into stroke-induced brain cavities by PLGA particles. Biomaterials. 2009; 30:2985–2994. [PubMed: 19278723]
10. Bible E, Dell'Acqua F, Solanky B, Balducci A, Crapo PM, Badylak SF, et al. Non-invasive imaging of transplanted human neural stem cells and ECM scaffold remodeling in the stroke-damaged rat brain by (19)F- and diffusion-MRI. Biomaterials. 2012; 33:2858–2871. [PubMed: 22244696]
11. Duncan K, Gonzales-Portillo GS, Acosta SA, Kaneko Y, Borlongan CV, Tajiri N. Stem cell-paved biobridges facilitate stem transplant and host brain cell interactions for stroke therapy. Brain Res. 2015; 1623:160–165. [PubMed: 25770817]
12. Bonnans C, Chou J, Werb Z. Remodelling the extracellular matrix in development and disease. Nat Rev Mol Cell Biol. 2014; 15:786–801. [PubMed: 25415508]
13. Medberry CJ, Crapo PM, Siu BF, Carruthers CA, Wolf MT, Nagarkar SP, et al. Hydrogels derived from central nervous system extracellular matrix. Biomaterials. 2013; 34:1033–1040. [PubMed: 23158935]
14. Crapo PM, Tottey S, Slivka PF, Badylak SF. Effects of biologic scaffolds on human stem cells and implications for CNS tissue engineering. Tissue Eng A. 2014; 20:313–323.
15. Badylak SF. Decellularized allogeneic and xenogeneic tissue as a bioscaffold for regenerative medicine: factors that influence the host response. Ann Biomed Eng. 2014; 42:1517–1527. [PubMed: 24402648]
16. Brown BN, Sicari BM, Badylak SF. Rethinking regenerative medicine: a macrophage-centered approach. Front Immunol. 2014; 5:510. [PubMed: 25408693]

Author Manuscript Author Manuscript Author Manuscript Author Manuscript

17. Sicari BM, Dziki JL, Siu BF, Medberry CJ, Dearth CL, Badylak SF. The promotion of a constructive macrophage phenotype by solubilized extracellular matrix. Biomaterials. 2014; 35:8605–8612. [PubMed: 25043569]
18. Dearth CL, Slivka PF, Stewart SA, Keane TJ, Tay JK, Londono R, et al. Inhibition of COX1/2 alters the host response and reduces ECM scaffold mediated constructive tissue remodeling in a rodent model of skeletal muscle injury. Acta Biomater. 2015
19. Piterina AV, Cloonan AJ, Meaney CL, Davis LM, Callanan A, Walsh MT, et al. ECM-based materials in cardiovascular applications: inherent healing potential and augmentation of native regenerative processes. Int J Mol Sci. 2009; 10:4375–4417. [PubMed: 20057951]
20. Agrawal V, Johnson SA, Reing J, Zhang L, Tottey S, Wang G, et al. Epimorphic regeneration approach to tissue replacement in adult mammals. Proc Natl Acad Sci U S A. 2010; 107:3351–3355. [PubMed: 19966310]
21. Beattie AJ, Gilbert TW, Guyot JP, Yates AJ, Badylak SF. Chemoattraction of progenitor cells by remodeling extracellular matrix scaffolds. Tissue Eng A. 2009; 15:1119–1125.
22. Massensini AR, Ghuman H, Saldin LT, Medberry CJ, Keane TJ, Nicholls FJ, et al. Concentration-dependent rheological properties of ECM hydrogel for intracerebral delivery to a stroke cavity. Acta Biomater. 2015; 27:116–130. [PubMed: 26318805]
23. Bible E, Chau DY, Alexander MR, Price J, Shakesheff KM, Modo M. Attachment of stem cells to scaffold particles for intra-cerebral transplantation. Nat Protoc. 2009; 4:1440–1453. [PubMed: 19798079]
24. Freytes DO, Martin J, Velankar SS, Lee AS, Badylak SF. Preparation and rheological characterization of a gel form of the porcine urinary bladder matrix. Biomaterials. 2008; 29:1630–1637. [PubMed: 18201760]
25. Saha K, Keung AJ, Irwin EF, Li Y, Little L, Schaffer DV, et al. Substrate modulus directs neural stem cell behavior. Biophys J. 2008; 95:4426–4438. [PubMed: 18658232]
26. Aurand ER, Wagner JL, Shandas R, Bjugstad KB. Hydrogel formulation determines cell fate of fetal and adult neural progenitor cells. Stem Cell Res. 2014; 12:11–23. [PubMed: 24141109]
27. Banerjee A, Arha M, Choudhary S, Ashton RS, Bhatia SR, Schaffer DV, et al. The influence of hydrogel modulus on the proliferation and differentiation of encapsulated neural stem cells. Biomaterials. 2009; 30:4695–4699. [PubMed: 19539367]
28. Farnebo S, Woon CY, Schmitt T, Joubert LM, Kim M, Pham H, et al. Design and characterization of an injectable tendon hydrogel: a novel scaffold for guided tissue regeneration in the musculoskeletal system. Tissue Eng A. 2014; 20:1550–1561.
29. Crapo PM, Gilbert TW, Badylak SF. An overview of tissue and whole organ decellularization processes. Biomaterials. 2011; 32:3233–3243. [PubMed: 21296410]
30. Marcal H, Ahmed T, Badylak SF, Tottey S, Foster LJ. A comprehensive protein expression profile of extracellular matrix biomaterial derived from porcine urinary bladder. Regen Med. 2012; 7:159–166. [PubMed: 22397606]
31. Crapo PM, Medberry CJ, Reing JE, Tottey S, van der Merwe Y, Jones KE, et al. Biologic scaffolds composed of central nervous system extracellular matrix. Biomaterials. 2012; 33:3539–3547. [PubMed: 22341938]
32. Taylor Z, Miller K. Reassessment of brain elasticity for analysis of biomechanisms of hydrocephalus. J Biomech. 2004; 37:1263–1269. [PubMed: 15212932]
33. Aurand ER, Wagner J, Lanning C, Bjugstad KB. Building biocompatible hydrogels for tissue engineering of the brain and spinal cord. J Funct Biomater. 2012; 3:839–863. [PubMed: 24955749]
34. Gefen A, Margulies SS. Are in vivo and in situ brain tissues mechanically similar? J Biomech. 2004; 37:1339–1352. [PubMed: 15275841]
35. Modo M, Stroemer RP, Tang E, Veizovic T, Sowniski P, Hodges H. Neurological sequelae and long-term behavioural assessment of rats with transient middle cerebral artery occlusion. J Neurosci Methods. 2000; 104:99–109. [PubMed: 11163416]
36. Modo M. Long-term survival and serial assessment of stroke damage and recovery – practical and methodological considerations. J Exp Stroke Transl Med. 2009; 2:52–68. [PubMed: 22389748]

Author Manuscript Author Manuscript Author Manuscript Author Manuscript

37. Stille M, Smith EJ, Crum WR, Modo M. 3D reconstruction of 2D fluorescence histology images and registration with in vivo MR images: application in a rodent stroke model. J Neurosci Methods. 2013; 219:27–40. [PubMed: 23816399]
38. Ashioti M, Beech JS, Lowe AS, Hesselink MB, Modo M, Williams SC. Multimodal characterisation of the neocortical clip model of focal cerebral ischaemia by MRI, behaviour and immunohistochemistry. Brain Res. 2007; 1145:177–189. [PubMed: 17320839]
39. Rossetti T, Nicholls F, Modo M. Intra-cerebral cell implantation: preparation and characterization of cell suspensions. Cell Transplant. 2015
40. Ito D, Tanaka K, Suzuki S, Dembo T, Fukuuchi Y. Enhanced expression of Iba1, ionized calcium-binding adapter molecule 1, after transient focal cerebral ischemia in rat brain. Stroke – J Cereb Circ. 2001; 32:1208–1215.
41. Aurand ER, Lampe KJ, Bjugstad KB. Defining and designing polymers and hydrogels for neural tissue engineering. Neurosci Res. 2012; 72:199–213. [PubMed: 22192467]
42. Simona BR, Hirt L, Demko L, Zambelli T, Voros J, Ehrbar M, et al. Density gradients at hydrogel interfaces for enhanced cell penetration. Biomater Sci. 2015; 3:586–591. [PubMed: 26222418]
43. Bjugstad KB, Lampe K, Kern DS, Mahoney M. Biocompatibility of poly(-ethylene glycol)-based hydrogels in the brain: an analysis of the glial response across space and time. J Biomed Mater Res A. 2010; 95:79–91. [PubMed: 20740603]
44. Fournier E, Passirani C, Montero-Menei CN, Benoit JP. Biocompatibility of implantable synthetic polymeric drug carriers: focus on brain biocompatibility. Biomaterials. 2003; 24:3311–3331. [PubMed: 12763459]
45. Ma Y, Wang J, Wang Y, Yang GY. The biphasic function of microglia in ischemic stroke. Prog Neurobiol. 2016
46. Mauney JR, Adam RM. Dynamic reciprocity in cell-scaffold interactions. Adv Drug Deliv Rev. 2015; 82–83:77–85.
47. Bracher M, Bezuidenhout D, Lutolf MP, Franz T, Sun M, Zilla P, et al. Cell specific ingrowth hydrogels. Biomaterials. 2013; 34:6797–6803. [PubMed: 23777918]
48. Plantman S. Proregenerative properties of ECM molecules. Biomed Res Int. 2013; 2013:981695. [PubMed: 24195084]
49. Meng FW, Slivka PF, Dearth CL, Badylak SF. Solubilized extracellular matrix from brain and urinary bladder elicits distinct functional and phenotypic responses in macrophages. Biomaterials. 2015; 46:131–140. [PubMed: 25678122]
50. Hosseini Y, Agah M, Verbridge SS. Endothelial cell sensing, restructuring, and invasion in collagen hydrogel structures. Integr Biol Camb. 2015; 7:1432–1441. [PubMed: 26379187]
51. Blakney AK, Swartzlander MD, Bryant SJ. The effects of substrate stiffness on the in vitro activation of macrophages and in vivo host response to poly(ethylene glycol)-based hydrogels. J Biomed Mater Res A. 2012; 100:1375–1386. [PubMed: 22407522]
52. Wolf MT, Dearth CL, Ranallo CA, LoPresti ST, Carey LE, Daly KA. Macrophage polarization in response to ECM coated polypropylene mesh. Biomaterials. 2014; 35:6838–6849. [PubMed: 24856104]
53. Keane TJ, Londono R, Turner NJ, Badylak SF. Consequences of ineffective decellularization of biologic scaffolds on the host response. Biomaterials. 2012; 33:1771–1781. [PubMed: 22137126]
54. Mokarram N, Merchant A, Mukhatyar V, Patel G, Bellamkonda RV. Effect of modulating macrophage phenotype on peripheral nerve repair. Biomaterials. 2012; 33:8793–8801. [PubMed: 22979988]
55. Brown BN, Valentin JE, Stewart-Akers AM, McCabe GP, Badylak SF. Macrophage phenotype and remodeling outcomes in response to biologic scaffolds with and without a cellular component. Biomaterials. 2009; 30:1482–1491. [PubMed: 19121538]
56. Roll L, Faissner A. Influence of the extracellular matrix on endogenous and transplanted stem cells after brain damage. Front Cell Neurosci. 2014; 8:219. [PubMed: 25191223]
57. Stabenfeldt SE, Munglani G, Garcia AJ, LaPlaca MC. Biomimetic microenvironment modulates neural stem cell survival, migration, and differentiation. Tissue Eng A. 2010; 16:3747–3758.

Author Manuscript Author Manuscript Author Manuscript Author Manuscript

58. Tate MC, Shear DA, Hoffman SW, Stein DG, Archer DR, LaPlaca MC. Fibronectin promotes survival and migration of primary neural stem cells transplanted into the traumatically injured mouse brain. Cell Transplant. 2002; 11:283–295. [PubMed: 12075994]

59. Hsiao TW, Tresco PA, Hlady V. Astrocytes alignment and reactivity on collagen hydrogels patterned with ECM proteins. Biomaterials. 2015; 39:124–130. [PubMed: 25477179]

60. Macaya DJ, Hayakawa K, Arai K, Spector M. Astrocyte infiltration into injectable collagen-based hydrogels containing FGF-2 to treat spinal cord injury. Biomaterials. 2013; 34:3591–3602. [PubMed: 23414684]

61. Georges PC, Miller WJ, Meaney DF, Sawyer ES, Janmey PA. Matrices with compliance comparable to that of brain tissue select neuronal over glial growth in mixed cortical cultures. Biophys J. 2006; 90:3012–3018. [PubMed: 16461391]

62. Leipzig ND, Shoichet MS. The effect of substrate stiffness on adult neural stem cell behavior. Biomaterials. 2009; 30:6867–6878. [PubMed: 19775749]

Author Manuscript Author Manuscript Author Manuscript Author Manuscript

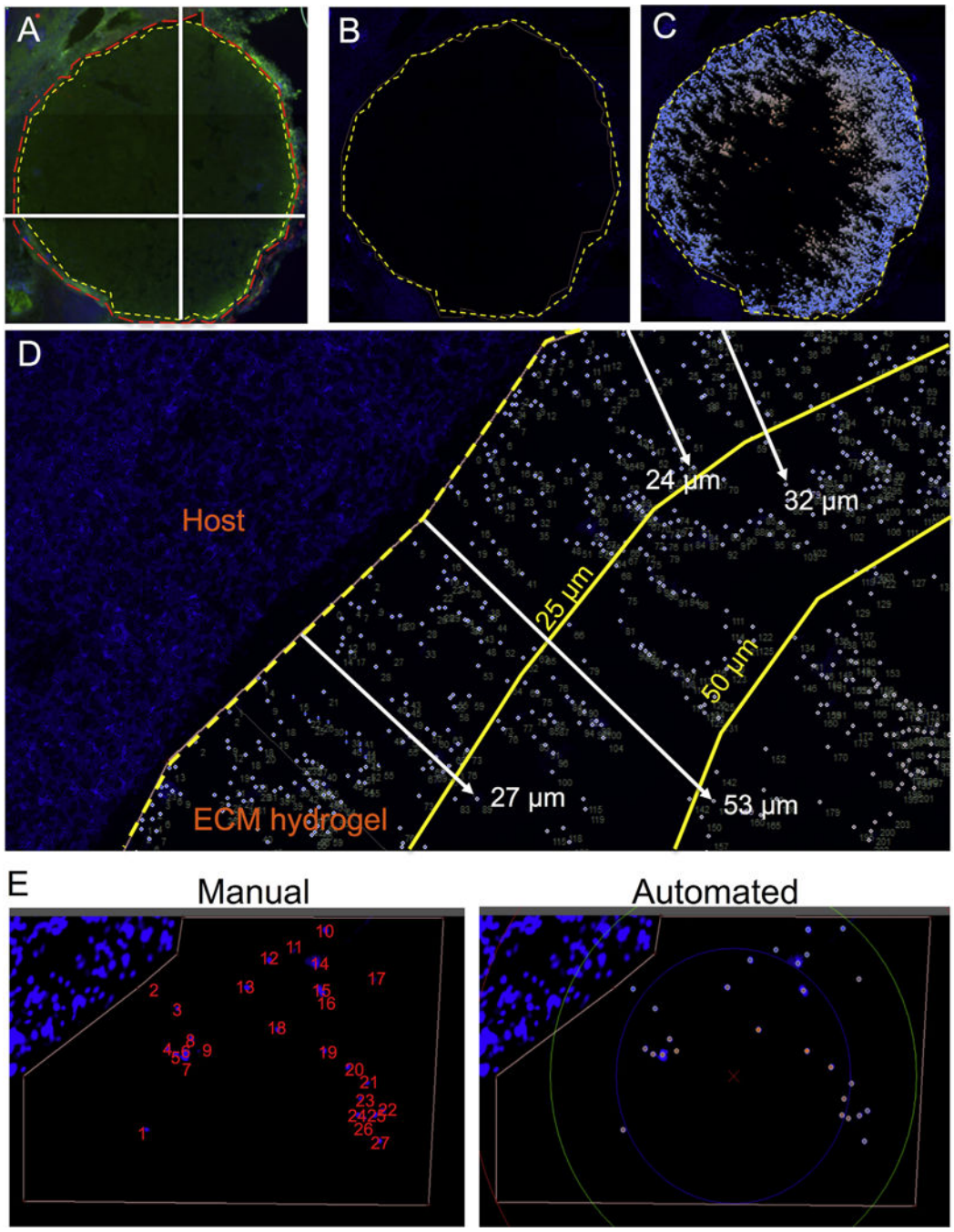

Fig. 1. Measuring cell infiltration

Overview of the cell infiltration quantification approach using Lux64R and DAPI stained fluorescent images. Using collagen I to stain the ECM biomaterial, the distinction between the lesion boundary and the ECM hydrogel interface is identified (**A**). Using Lux64R, the lesion boundary is then drawn and defined (**B**). The cells inside the boundary are then labeled and counted (**C**). A closer view in a region of interest shows that each cell is accurately identified and labeled, while measuring its distance traveled from the previously

Author Manuscript Author Manuscript Author Manuscript Author Manuscript

defined lesion boundary (**D**). Manual and automated cell counts using Lux64R shows cells being correctly identified for quantification of cell invasion (**E**).

Author Manuscript Author Manuscript Author Manuscript Author Manuscript

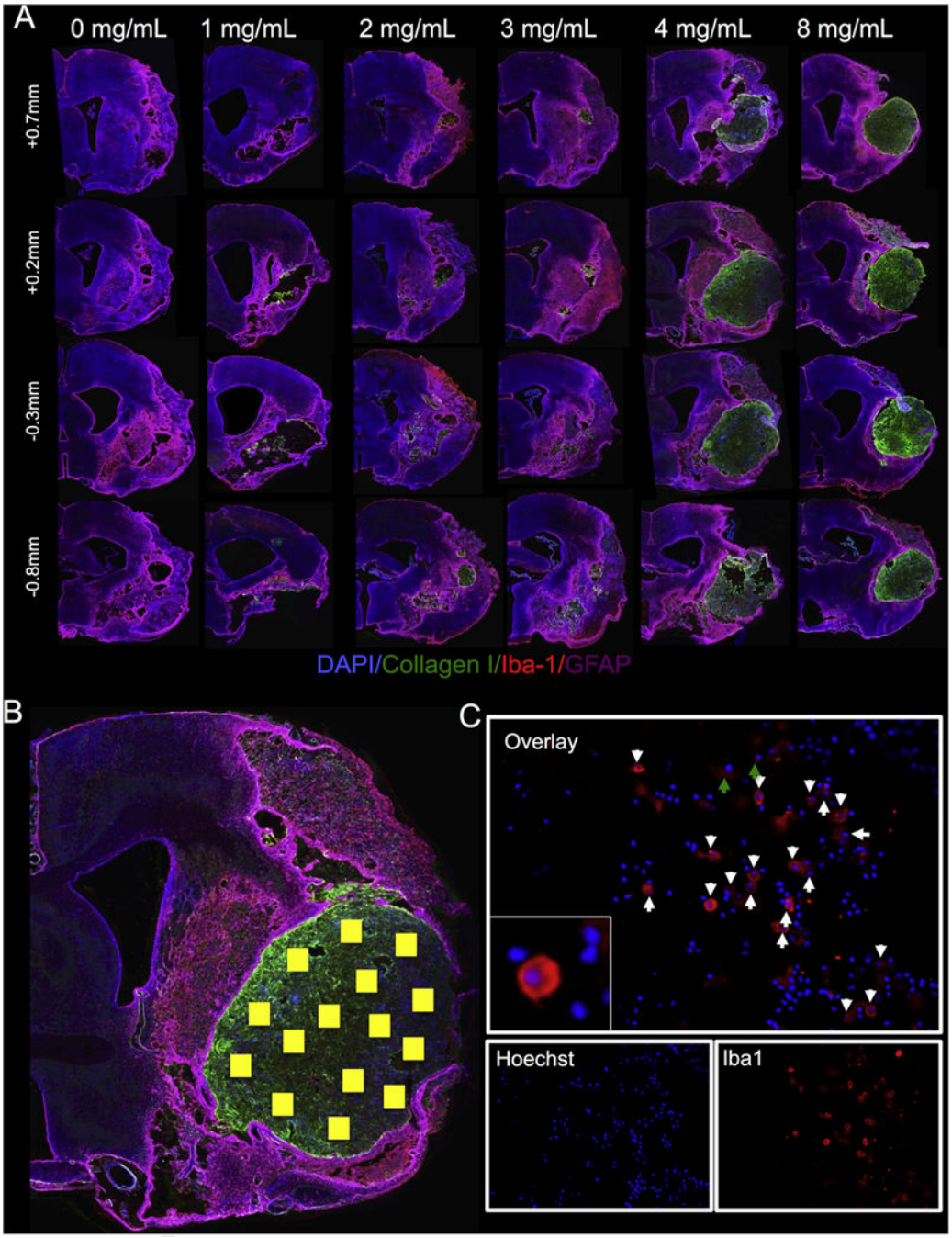

Fig. 2. Concentration-dependent retention of ECM hydrogel in the lesion cavity

(**A**) Whole hemisphere images show the gelation and retention properties of the injected ECM hydrogel at different concentrations. Since collagen I is more abundant in the ECM contains compared to the host brain tissue, it can be used for histological visualization of the injected material. A vehicle injection (0 mg/mL) of PBS indicated no collagen I detection inside the lesion cavity. At 1 and 2 mg/mL, the ECM material mostly permeated into the brain tissue, whereas at 3 mg/mL, hydrogel formed and was retained in the cavity with some permeation into the host tissue. At concentrations greater than 3 mg/mL, the ECM material

Author Manuscript Author Manuscript Author Manuscript Author Manuscript

shows gelation with little to no signs of permeation into the peri-infarct tissue, retaining both its morphology, as well as its shape. In order to accurately characterize the invading cells, multiple images were acquired inside the ECM material (as shown by the yellow boxes) (**B**). Once the images were acquired, manual counts of DAPI indicated the total number of cells in the field of view and co-staining with another marker (Iba-1 in this case) would result in characterization of the invading cells (as shown with white arrows) (**C**). (For interpretation of the references to color in this figure legend, the reader is referred to the web version of this article.)

Author Manuscript Author Manuscript Author Manuscript Author Manuscript

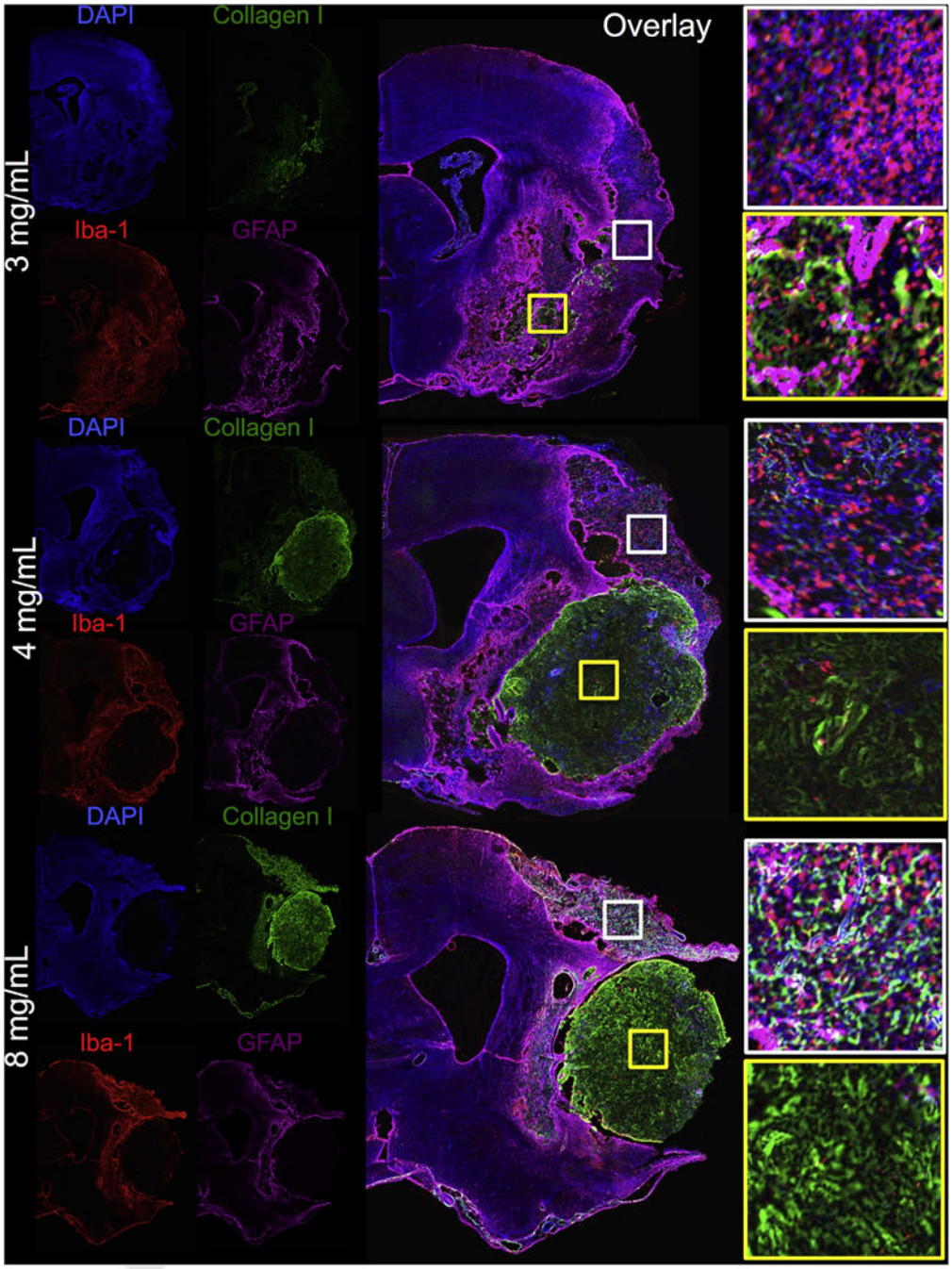

Fig. 3. Interface between ECM hydrogel and host tissue

Concentrations >3 mg/mL resulted in an in situ gelation and retention within the lesion cavity producing an interface where the ECM hydrogel contacts with the host brain tissue. It is important to note two typical microenvironments within which ECM material can be found in these stroke-damaged brains: 1. The lesion cavity (yellow boxes); 2. Severely damaged tissue that is not part of the lesion core (white boxes). Higher concentrations of 4 and 8 mg/mL typically completely filled the cavity, but also displaced some damaged tissue. The 3 mg/mL also permeated into damaged tissue directly adjacent to the cavity. In areas of

Author Manuscript Author Manuscript Author Manuscript Author Manuscript

cortical tissue damage, some permeation of ECM could be seen. These areas were mostly void of neurons, but significant amounts of microglia were present directly interacting with some of the permeating ECM. (For interpretation of the references to color in this figure legend, the reader is referred to the web version of this article.)

Author Manuscript Author Manuscript Author Manuscript Author Manuscript

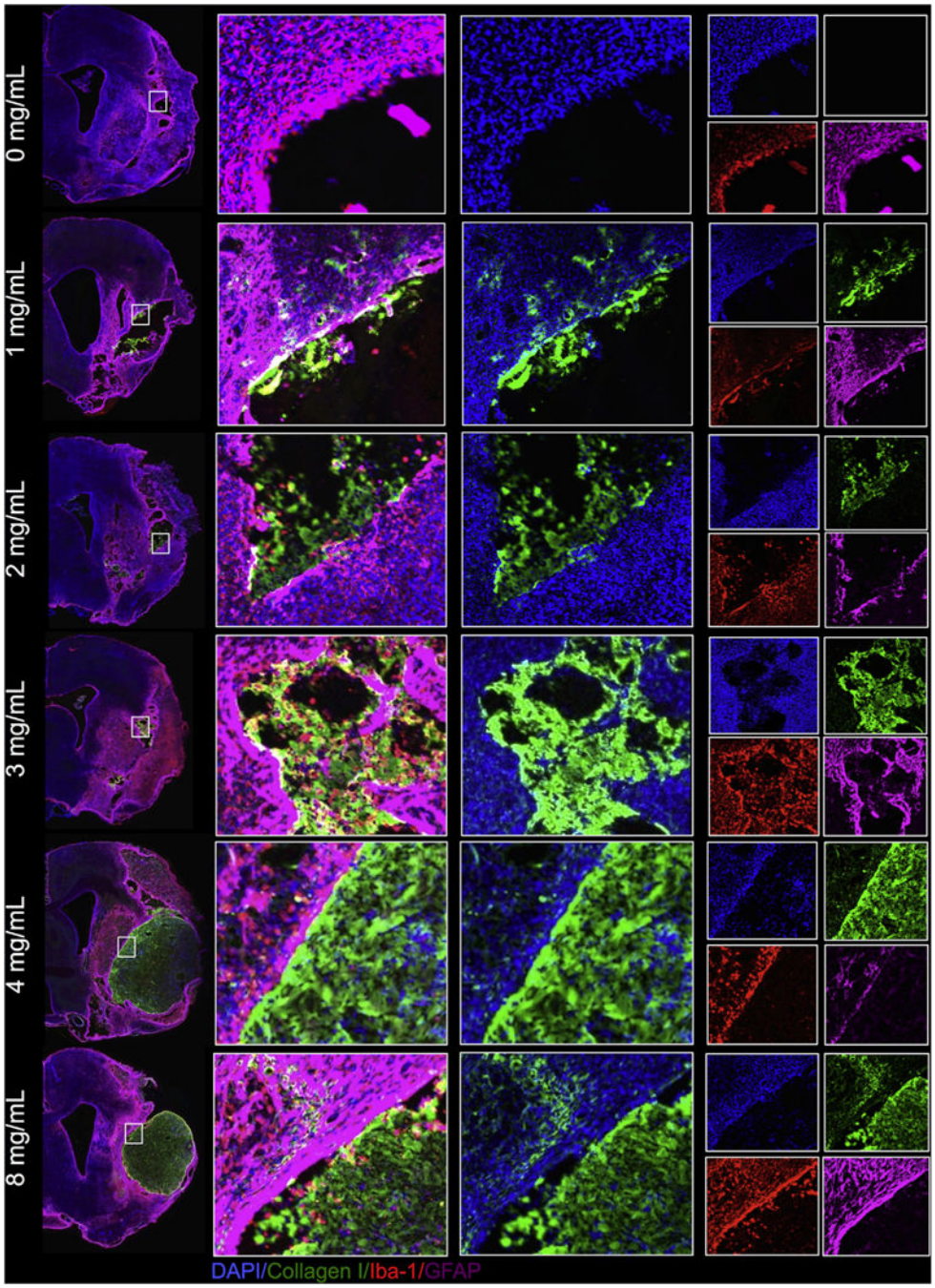

Fig. 4. Gelation and permeation of the ECM material at the host tissue interface

At 0 mg/mL (PBS injection), no exogenous collagen I is detected inside the lesion cavity (as delineated by Iba-1 staining for microglia and GFAP for astrocytes). At 1 and 2 mg/mL, injected ECM material shows poor retention inside the lesion cavity, as significant diffusion of the ECM material into the peri-infarct area can be seen. At 3 mg/mL, the ECM material shows hydrogel formation and retention inside the cavity, with some diffusion into the surrounding tissue. At 4 and 8 mg/mL, a clear boundary can be seen at the interface between the host tissue and the ECM hydrogel. Concentrations >3 mg/mL resulted in complete

Author Manuscript Author Manuscript Author Manuscript Author Manuscript

gelation and retention of the hydrogel with minimal to no diffusion into the host tissue. The predominant cell phenotypes surrounding all cavities consist of microglia and astrocytes with evidence of cell invasion of these host cells into the injected material at all concentrations.

Author Manuscript Author Manuscript Author Manuscript Author Manuscript

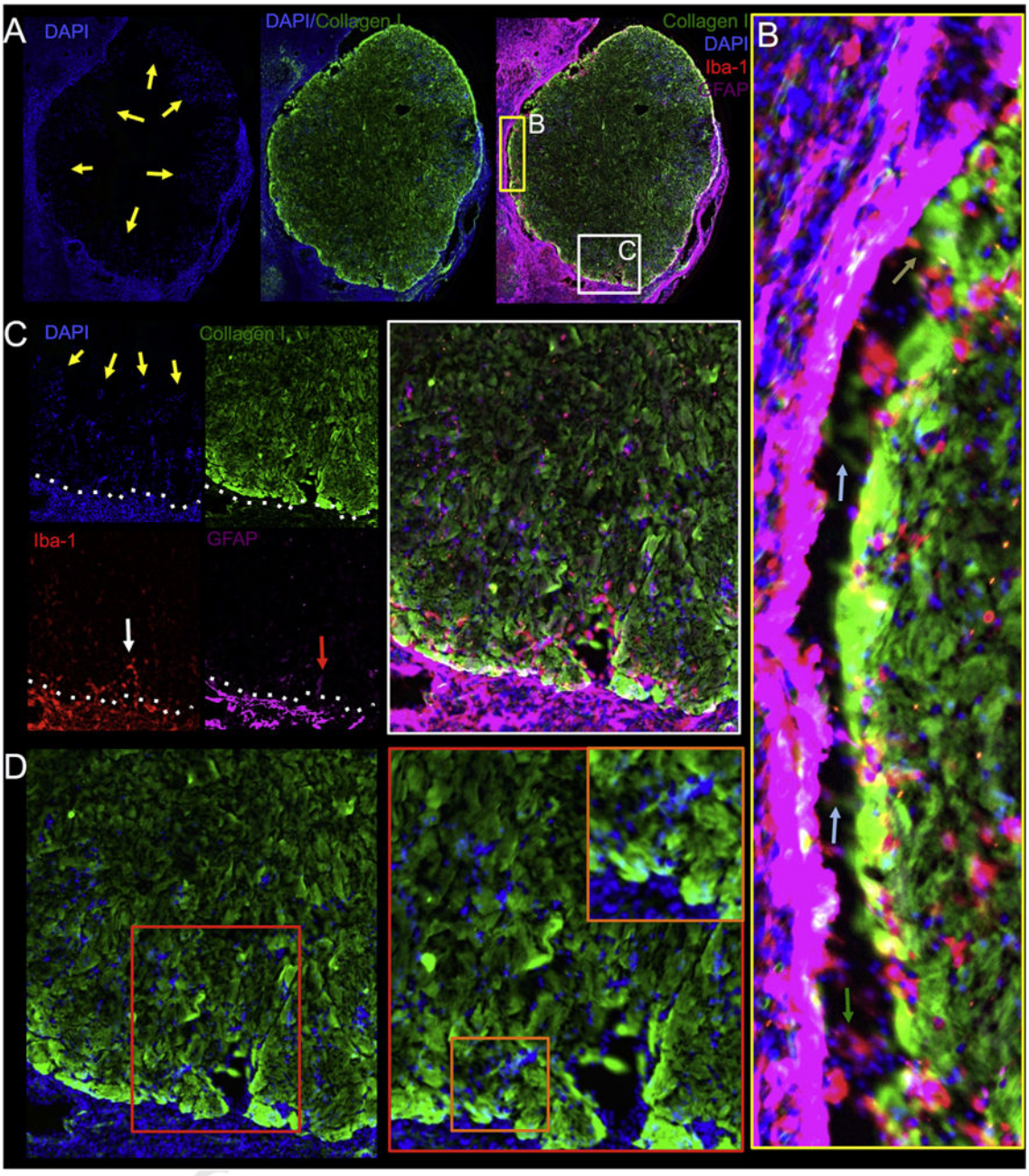

Fig. 5. Patterns of cell invasion

A microscopic view of the lesion interface with the ECM hydrogel (collagen I+ area) indicates a higher density of DAPI+ cells surrounding the biomaterial with evidence of a concentric invasion of host cells (yellow arrows) into the acellular material. The predominant cellular phenotypes surrounding the ECM hydrogel, forming the glia limitans, are astrocytes (GFAP+ cells) and microglia (Iba-1+ cells). The injection-drainage approach produces a consistent coverage of the cavity (**A**). A magnified view of the interface between the host tissue and the ECM hydrogel reveals invading microglia migrating from the host tissue to the hydrogel (green arrow). A collagen I negative staining area in some edge

Author Manuscript Author Manuscript Author Manuscript Author Manuscript

regions of the host-biomaterial interface was also evident (blue arrows), but this did not affect the invasion of some cells, although a close interface between host and hydrogel dramatically facilitated cell invasion (brown arrow) (**B**). In order for the cells to migrate into the damaged tissue, a structural support for the attachment and survival of the cells is favorable. Most commonly microglia are the cells that infiltrated the furthest into the hydrogel, whereas astrocytes were mostly present closer to the host tissue (**C**). Indeed, a guided chain-like migration along collagen I negative channels can be seen into the hydrogel, potentially indicating that hydrogel ultrastructure is also a contributing factor for initial cell invasion (**D**). (For interpretation of the references to color in this figure legend, the reader is referred to the web version of this article.)

Author Manuscript Author Manuscript Author Manuscript Author Manuscript

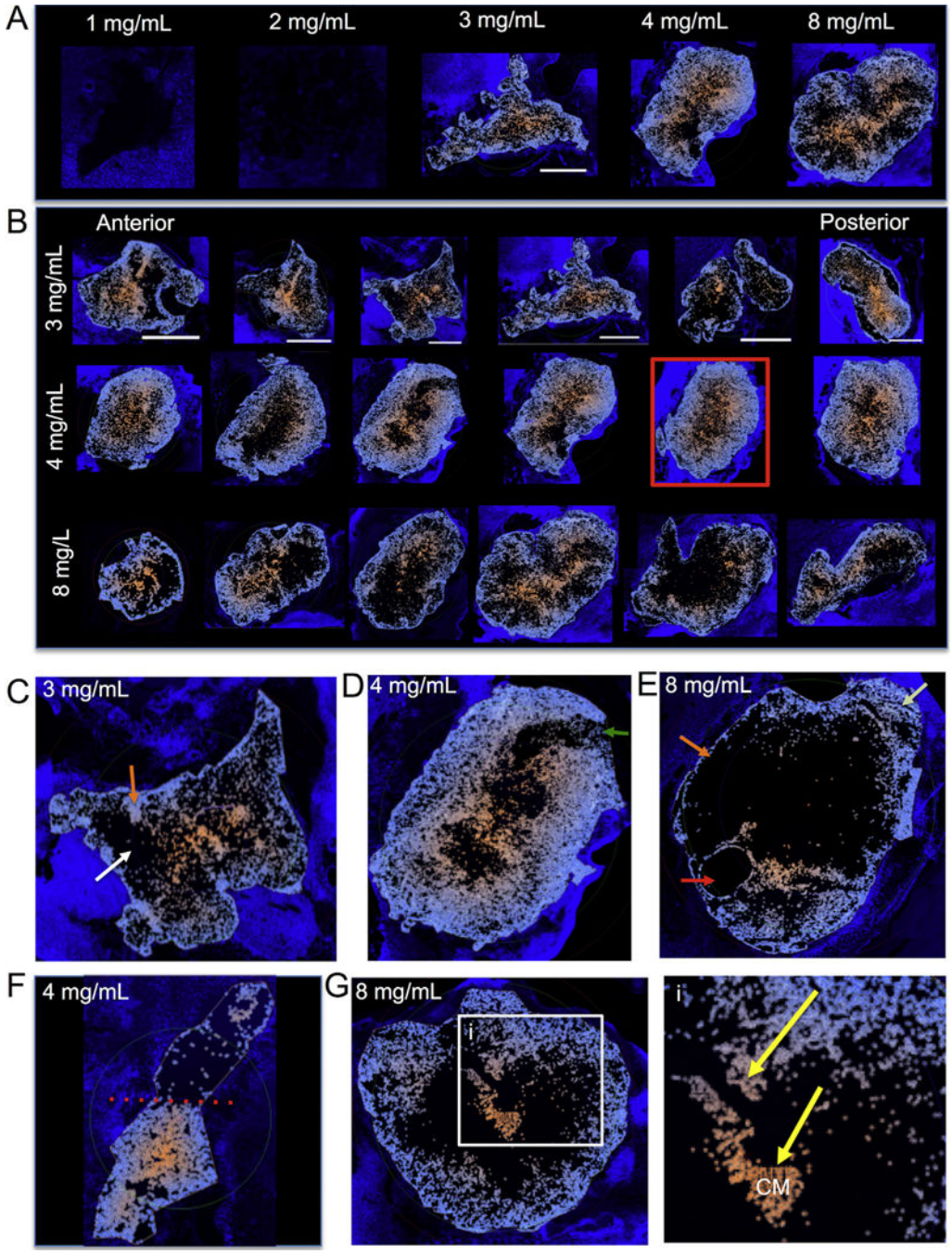

Fig. 6. Cell invasion – Colorimetric maps

Identification and labeling of cell invasion at different concentrations using Lux64R based on DAPI staining within a collagen I outline ROI. Using a colorimetric method ranging from light blue (closest to the host boundary) to orange (furthest from host boundary), maps of cell invasion were created to highlight differences between ECM concentrations (**A**). These maps also allowed us to inspect the anterior-posterior invasion of cells within the ECM hydrogel. It was evident here that the smaller ECM hydrogel areas found at the poles of the cavity saw a more complete coverage of cell invasion compared to more central slices which

Author Manuscript Author Manuscript Author Manuscript Author Manuscript

occupied a large area (**B**). Invasion typically followed a concentric pattern that saw cells migrating to the center of mass of the injected ECM hydrogel, in some cases leading to very homogenous distribution of host cells through the material (red box). Nevertheless, important qualitative differences in cell invasion were also noted on these colorimetric maps. Cell invasion in some instance followed a very densely packed channel with blind spots within the material hardly seeing any invasion (**C**). In other cases, there was a no significant invasion (green arrow) in a very restricted region suggesting that potential host factors, such as scarring can influence invasion (**D**). Indeed, the varied pattern of invasion or the lack therefore indicates that technical factors, such as an air bubble (red arrow), as well as poor interface with host tissue (orange arrow) influence cell invasion, even though other areas of the gel are efficiently invaded (light green arrow) (**E**). The differential patterns of cell invasion into the same hydrogel hence strongly suggest that the host microenvironment surround the ECM material has a significant influence on cell invasion (**F**). Nevertheless even if there are blind spots within the hydrogel and areas of poor cell invasion at the host-gel interface, invading cells will find channels (yellow arrows) to move towards the center of mass (**i**) and are likely to continue their migration in the absence of encountering other cells (**G**). Scale bars are 5000 μm. (For interpretation of the references to color in this figure legend, the reader is referred to the web version of this article.)

Author Manuscript Author Manuscript Author Manuscript Author Manuscript

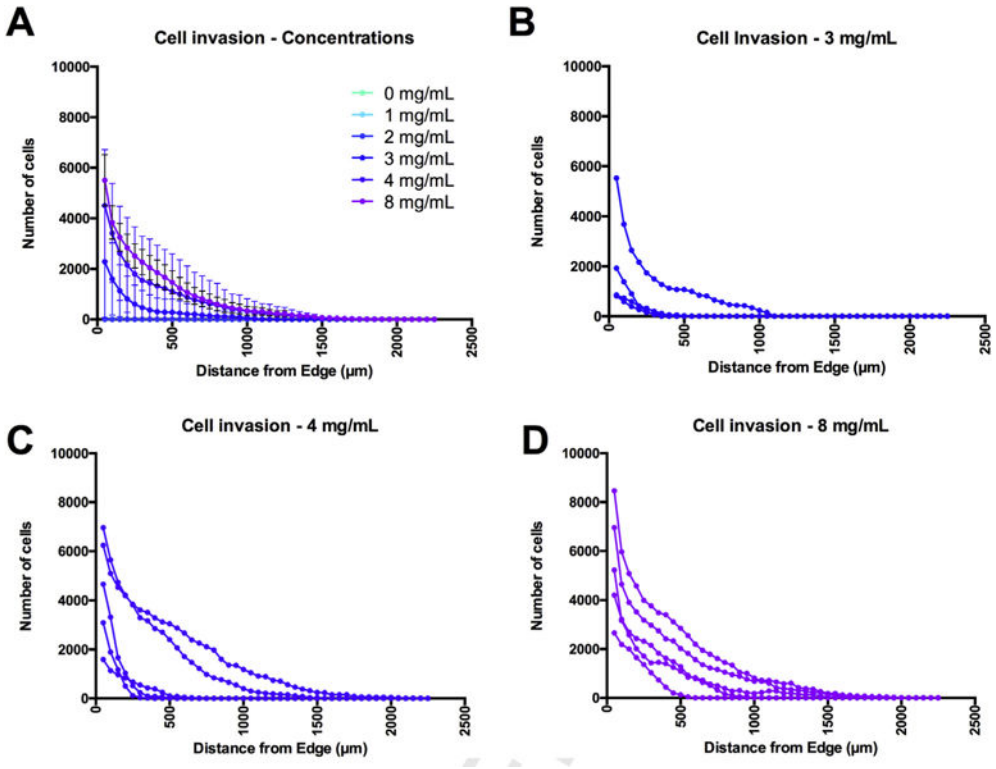

Fig. 7. Cell invasion – Quantification

(**A**) Quantification of the cell infiltration into the infarct cavity afforded a comparison of all ECM concentration (mean ± standard deviation) to determine how many cells invaded each 25 μm concentric circle from the center of the mass, as well as the total distance of invasion in relation to the ECM's interface with host tissue. Mapping of individual animals revealed a spread of cell invasion reflecting difference in the interface between host and ECM hydrogel, as well as ECM concentration for 3 mg/mL (**B**), 4 mg/mL (**C**) and 8 mg/mL (**D**).

Author Manuscript Author Manuscript Author Manuscript Author Manuscript

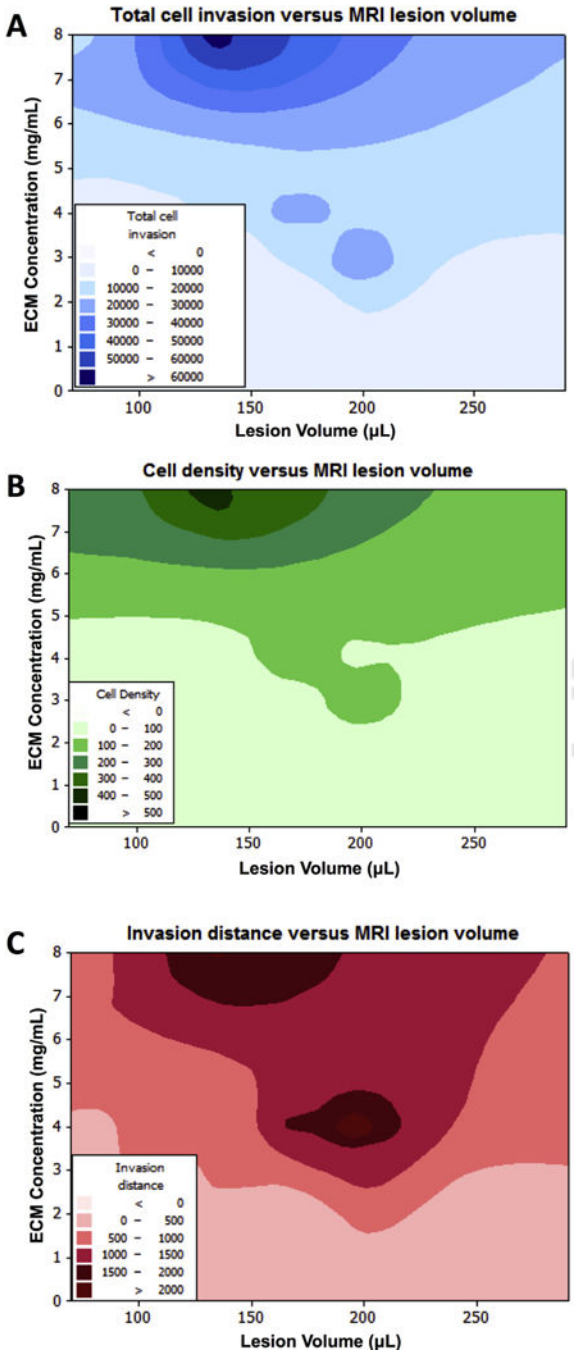

Fig. 8. Contour plots

To determine an interaction between ECM concentration and lesion volume on the number of cells invading the ECM (**A**), cell density within the ECM material (**B**), as well as the distance of cell invasion (**C**), contour plots were generated to illustrate which combinations would be the most and least combinations.

Author Manuscript Author Manuscript Author Manuscript Author Manuscript

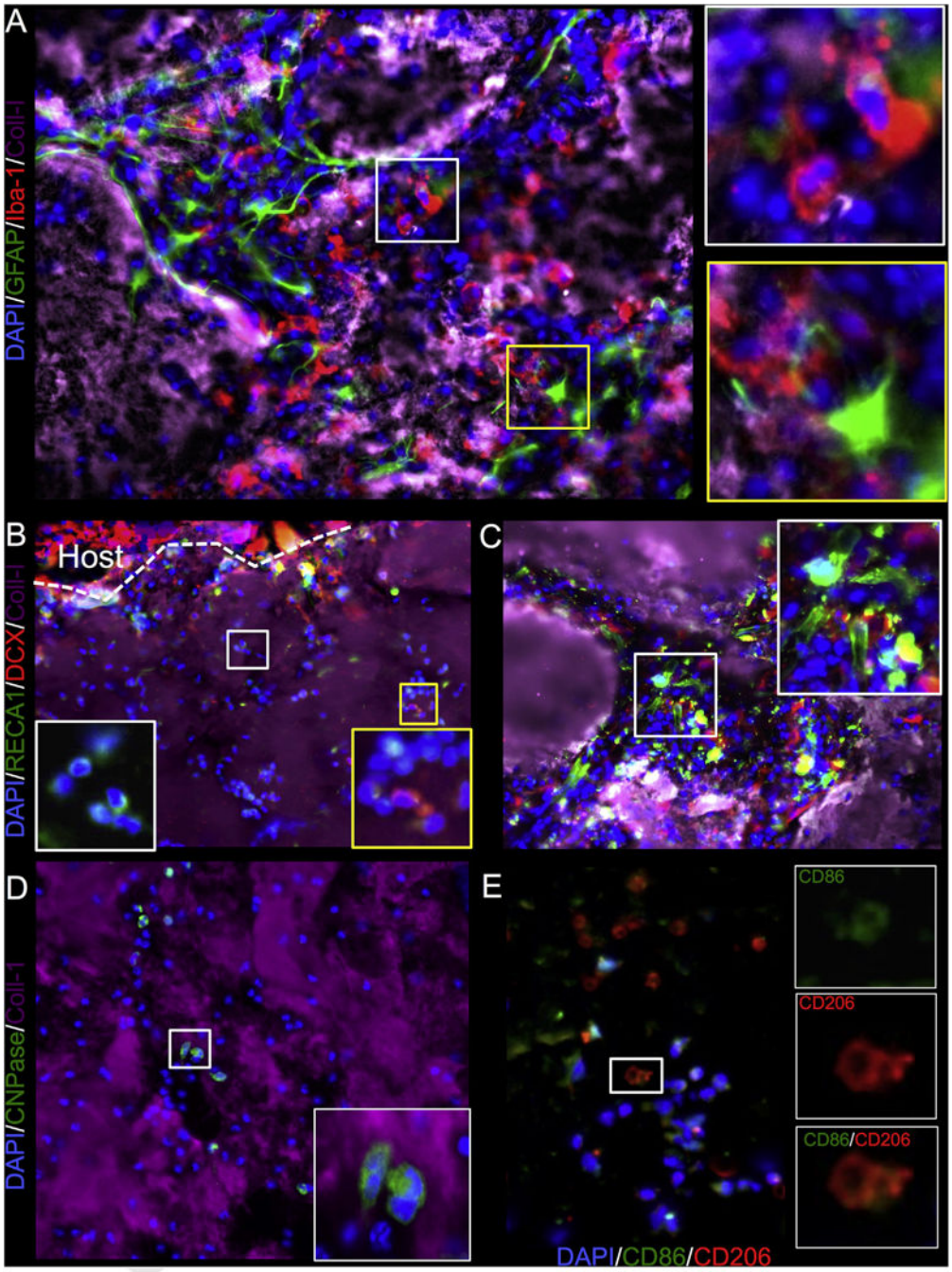

Fig. 9. Cell invasion – phenotypic characterization

Phenotypic characterization of cell invasion into injected ECM (collagen I+ area) was focused on cell phenotypes found in the brain: neural progenitors as revealed by doublecortin (DCX+), oligodendrocytes (CNPase+), astrocytes (GFAP), microglia (Iba-1+) and endothelial cells (RECA-1+). There was noted invasion of microglia with a bulbar morphology pioneering a path for astrocytes to follow (**A**). A significant number of DCX+ neural progenitors also invaded the ECM, presumably these were already responding to the surrounding tissue damage (**B**). A smaller number of endothelial cells were seen invading

Author Manuscript Author Manuscript Author Manuscript Author Manuscript

the ECM material. However, in some cases endothelial cells appeared to organize into tubules, but this was typically in areas where there were remnants of damaged tissue that were engulfed by the ECM hydrogel (**C**). Oligodendrocytes were also found to invade deep into the ECM material, but cells were mostly of an uncharacteristic bulbar shape (**D**). In addition to the “indigenous” brain cells, the infiltration of peripheral macrophages and their polarization towards an M1 (CD86+) or M2 (CD206+) phenotype were investigated (**E**). Almost all CD206+ cells were also positive for CD86.

Author Manuscript Author Manuscript Author Manuscript Author Manuscript

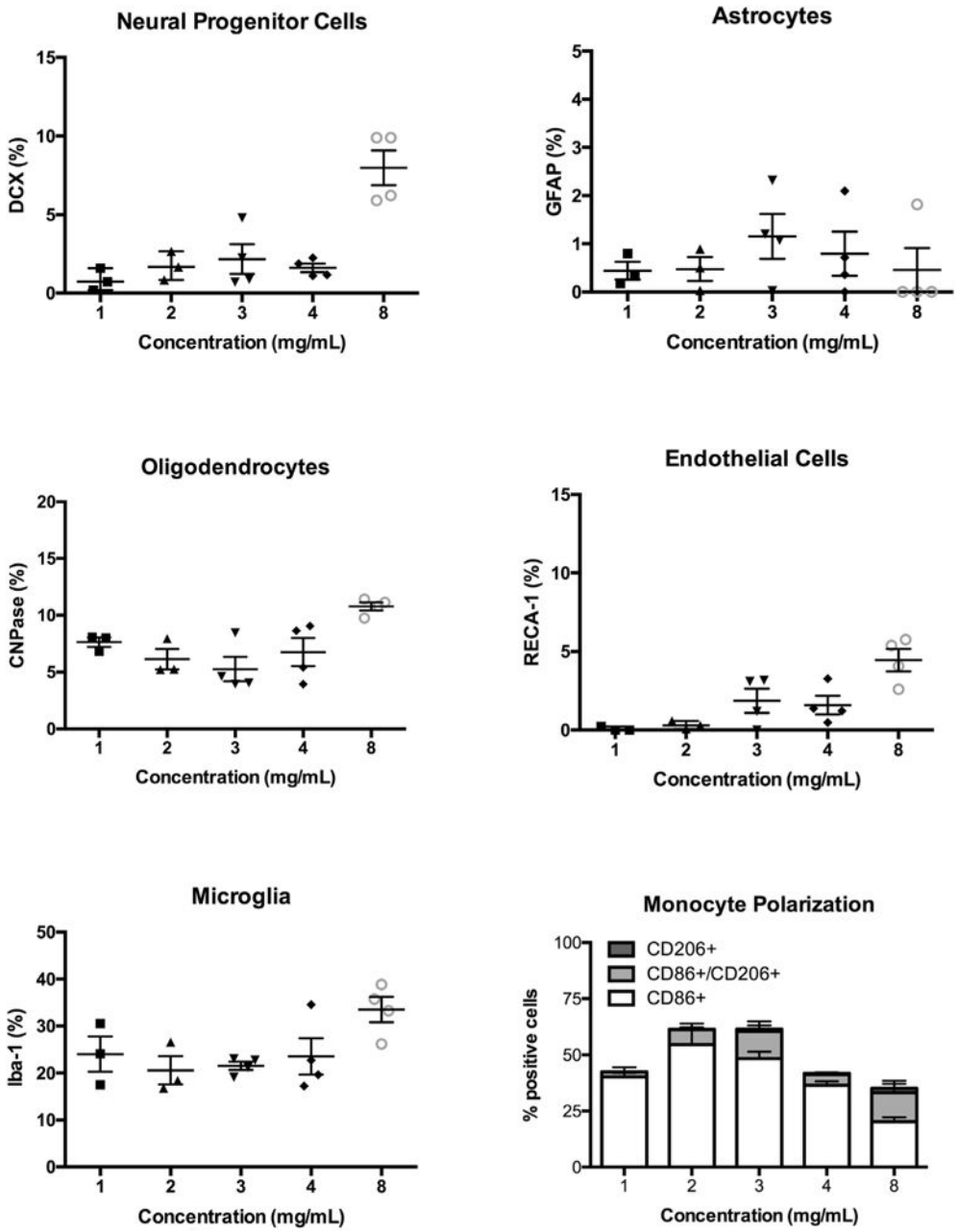

Fig. 10. Cell invasion – Quantification of cell phenotypes

An 8 mg/mL ECM concentration resulted in the most significant proportion of brain cells invading the material. Most significantly neural (DCX+ cells) and oligodendrocyte progenitors (CNPase+ cells) were among the first phenotypes to invade the ECM, with astrocytes (GFAP+ cells) and endothelial (RECA-1+) cells being most negligible proportions. Nevertheless, as expected a high proportion of microglia (IBa-1+ cells) and macrophages invaded the material. Again, an 8 mg/mL ECM concentration produced the most significant shift from a M1 (CD86+ cells) towards an M2 (CD206+ cells) phenotype.